Published in final edited form as:
Development. 2004 January ; 131(2): . doi:10.1242/dev.00944.

Both Cyclin B levels and DNA-replication checkpoint control the early embryonic mitoses in *Drosophila*

Jun-Yuan Ji[1], **Jayne M. Squirrell**[2], and **Gerold Schubiger**[1,*]

[1]Department of Biology, University of Washington, Seattle, WA 98195-1800, USA

[2]Laboratory of Molecular Biology, University of Wisconsin, Madison, WI 53706, USA

Summary

The earliest embryonic mitoses in *Drosophila*, as in other animals except mammals, are viewed as synchronous and of equal duration. However, we observed that total cell-cycle length steadily increases after cycle 7, solely owing to the extension of interphase. Between cycle 7 and cycle 10, this extension is DNA-replication checkpoint independent, but correlates with the onset of Cyclin B oscillation. In addition, nuclei in the middle of embryos have longer metaphase and shorter anaphase than nuclei at the two polar regions. Interestingly, sister chromatids move faster in anaphase in the middle than the posterior region. These regional differences correlate with local differences in Cyclin B concentration. After cycle 10, interphase and total cycle duration of nuclei in the middle of the embryo are longer than at the poles. Because interphase also extends in checkpoint mutant (*grapes*) embryo after cycle 10, although less dramatic than wild-type embryos, interphase extension after cycle 10 is probably controlled by both Cyclin B limitation and the DNA-replication checkpoint.

Keywords

Early embryonic mitosis; Cdk1-CycB; *Drosophila*; Metaphase; Interphase

Introduction

Timing and coordination of biological processes are crucial for normal cellular function and development. For example, cell-cycle events that occur at the wrong time can result in abnormal development and lead to disease states such as cancer (Sherr, 1996; Zou et al., 1999). Early embryonic cycles provide a good system for analyzing such timing mechanisms. After fertilization, the earliest embryonic divisions are rapid, synchronous and maternally controlled in many organisms. These early cycles exhibit only S and M phases, essentially a stripped-down version of the complete somatic cycles (Murray, 1991). Indeed, the feedback loop in which Cdk1-cyclin and anaphase-promoting complex inactivate each other is simpler in early embryonic cycles compared with somatic cell cycles (Morgan and Roberts, 2002).

Studies of early developmental events in *Xenopus* have identified at least two important temporal phases. First, timing of the early synchronous cycles is based on oscillation of Cdk1-CycB activity (Murray and Kirschner, 1991). Second, later cell cycles slow down and become asynchronous, depending on the nucleo-cytoplasmic ratio (Newport and Kirschner, 1982; Kirschner et al., 1985). This transition point for both cell-cycle rate and synchrony is

*Author for correspondence (gerold@u.washington.edu).

known as mid-blastula transition (Yasuda and Schubiger, 1992). As in *Xenopus*, the nucleo-cytoplasmic ratio also regulates the cell-cycle rate in *Drosophila* embryos (Edgar et al., 1986). However, loss of synchrony does not occur at a single time point during the syncytial blastoderm cycles (cycle 10-13) in *Drosophila* embryos (Foe and Alberts, 1983). Similarly, zygotic gene transcription begins gradually and as early as cycle 8 in a gene-specific manner (Pritchard and Schubiger, 1996). During this maternal-zygotic transition, depletion of mitotic cyclins might cause the elongation of interphase, thus permitting sufficient time for zygotic transcription to proceed (Edgar and Datar, 1996; Shermoen and O'Farrell, 1991).

Over the last 60 years, many studies have analyzed the timing of the first 13 cycles in *Drosophila* using two different approaches. First, embryos were fixed at different times and stained to estimate the duration of both the total cell cycle and cycle phases based on the percentages of embryos in each specific cycle phase. Second, time-lapse recordings of living embryos were made using either DIC or confocal microscopy. The former approach generated variable, thus potentially unreliable, results. For example, metaphase length before cycle 10 was estimated as between 0.3 and 0.7 minutes by Rabinowitz (Rabinowitz, 1941) and between 2.0 and 2.4 minutes by Stiffler et al. (Stiffler et al., 1999). Although the latter method is useful for estimating total cell-cycle length, the duration of cycle phases cannot be defined because chromosomal morphology is not discernable with DIC optics. Although time-lapse recordings of embryos labeled with fluorescent markers using confocal microscopy have been used to analyze interphase and total cell-cycle time of cycles 11-13 (Sibon et al., 1997; Yu et al., 2000), this method is ineffective for imaging nuclei prior to their migration to the cortex (cycle 10). In addition, long-term imaging with standard confocal wavelengths is detrimental to living embryos (Squirrell et al., 1999). These limitations result in a significant gap in our understanding of the specific timing of cell-cycle events during the early embryonic cycles, particularly those before cycle 10.

Two-photon laser-scanning microscopy (TPLSM) circumvents the technical problems mentioned above, as it permits high resolution imaging deep within thick, light-scattering tissues (Centonze and White, 1998), as well as long-term imaging of living specimens (Squirrell et al., 1999). Here, by using TPLSM, we characterize cell-cycle progression of preblastoderm cycles (before cycle 10) and compare it with syncytial blastoderm cycles (after cycle 10) in live embryos. Furthermore, we show that crucial CycB concentrations control both interphase duration and the timing of metaphase-anaphase transition.

Materials and methods

Fly strains

Drosophila melanogaster strains were maintained on standard cornmeal-yeast agar medium at 25°C. We used *Sevelen* flies as wild-type control (+), which is also the genetic background for all the flies used in this study. Stocks with varied gene doses of maternal *cycB* were provided by Christian Lehner (Jacobs et al., 1998) and their embryos were referred by the same nomenclature as previously described (Ji et al., 2002). A transgenic line expressing a fusion protein of histone H2Av and green fluorescent protein (referred to as histone-GFP) was obtained from Robert Saint (Clarkson and Saint, 1998). For live imaging, '*one cycB*' embryos refer to embryos from *w*/+; $cycB^{-}/cycB^{+}$; *histone-GFP*/+ females, '*two cycB*' (wild type) embryos are from +; $cycB^{+}/cycB^{+}$; *histone-GFP*/+ females, and '*four cycB*' embryos are from *w*/+; $cycB^{+}/cycB^{+}$, *CyO*; $2P[w^{+}\ cycB^{+}]$/*histone-GFP* females. William Sullivan provided us the null allele *grapes*^{1} (grp^{1}) (Fogarty et al., 1997; Sullivan et al., 1993). Female flies with grp^{1}/grp^{1}; *histone-GFP* genotype were generated through standard genetic crosses from grp^{1}/CyO and *histone-GFP* flies and their embryos were referred as grp^{1} embryo (Fig. 1J).

Egg collection and fixation protocols

For all egg collections, flies were put on new food for 1 hour at 25°C, then placed on agar plates with yeast paste for three times, 30 minutes each time, to purge the females of over-aged embryos. For live imaging, embryos expressing histone-GFP (from homozygotic transgenic females) were collected on agar plates for 15 minutes and aged for 20-30 minutes. For mitotic index analyses, embryos were collected for 90 minutes then fixed immediately. The fixation and immunostaining protocols were performed as described by Stiffler et al. (Stiffler et al., 1999) and Ji et al. (Ji et al., 2002).

Two-photon laser scanning microscopy (TPLSM)

Embryos were manually dechorionated and lined up on a 22×30 mm gluey cover glass (Schubiger and Edgar, 1994). This cover glass was then taped to a plastic holder that resembled a 25×76 mm glass slide with a 20×26 mm hole cut in the center. To prevent dehydration, we covered embryos with a thin layer of halocarbon oil (HC-700, Halocarbon Products Corp.), which is oxygen permeable.

The two-photon imaging was performed on a BioRad Radiance 2000 System equipped with a Mai Tai laser (Spectra Physics) set at 900 nm and a Nikon Eclipse E600FN microscope with a 40×/1.3 Nikon Plan Apo oil objective. Four-dimensional data were collected using Direct Detection System and LaserSharp software (BioRad) with the zoom set at 1.7. Single slow scans of two optical sections (5 μm apart) were taken every 10 seconds. The images were compiled into time-lapse recordings using 4D Turnaround-Java software (Thomas et al., 1996) and then analyzed with 4D Viewer software (Thomas et al., 1996).

Embryos were imaged for up to 2 hours. The room temperature was 21.6±0.4°C (n=21 days). We were able to detect the histone-GFP signal as early as cycle 4. Two hours of laser scanning did not reduce the hatching rates: 86% of the imaged embryos hatched (n=21 randomly chosen embryos) compared with 89% in non-imaged histone-GFP control embryos (n=210). Time-lapse recordings from unhatched embryos were not used.

A two-photon optical workstation was used to generate bright field transmission images (Fig. 6A,B). This transmitted light imaging is achieved by simply allowing the scanning infrared laser beam (900 nm) to pass through the live embryo and detecting it by an infrared photodiode (Wokosin et al., 2003).

Estimation of cell-cycle-phase duration with fixed embryos

Fixed embryos were labeled with an antibody against histone H1 and an antibody against phosphorylated histone H3. Because histone H3 is phosphorylated at Ser10 at the beginning of prophase, while the dephosphorylation is initiated at anaphase and completed at the end of telophase (Hendzel et al., 1997; Su et al., 1998; Wei et al., 1999), this double staining method enabled us to clearly distinguish interphase and the different mitotic phases. The nomenclature and mitotic phases of early embryonic cycles were according to Foe et al. (Foe et al., 1993). Embryos were analyzed with a Nikon Microphot-FX fluorescence microscope using a 20× objective.

With fixed embryos, the duration of a cell-cycle phase was estimated as the percentage of embryos in the cell-cycle phase within a specific cycle. This fraction, also known as the mitotic index, represents the percentage of the total cell-cycle time spent in that phase. The total cell cycle duration for a given cycle was determined from the TPLSM recordings, thus the time of the cell-cycle phase could be calculated. To obtain meaningful estimations, several hundred embryos of each cell cycle were analyzed. The results were analyzed with

the exact distribution of Wilcoxon-Mann-Whitney statistic test (StatXact 4.0 by Cytel Software).

CycB quantification

We collected images of embryos immunostained with the anti-CycB antiserum Rb271 (Whitfield et al., 1990) using a BioRad MRC-600 confocal microscope system as described in Stiffler et al. (Stiffler et al., 1999). Images of mid-sections through each nucleus were obtained with an Olympus microscope using a 60× oil objective and the confocal settings of Zoom 3.0 and Kalman 6. To outline energids (Fig. 3A), we used StackViewer, software written by Eli Meir (http://www.beakerware.org/stackviewer). With the same software we calculated the average pixel intensity of each energid.

To compare relative CycB levels within embryos, each embryo was divided into three regions: anterior, middle and posterior (Fig. 3). The average pixel intensity of CycB staining of three different energids in each region was measured. For each embryo, the mean values of the three energids in each region were calculated, representing the CycB level in that region. We compared the relative CycB concentration in the three regions by assigning ranks for each region: the lowest CycB region is ranked 1, intermediate level ranked 2 and the highest ranked 3. The rank sum in different cell-cycle phases (Fig. 3E) was statistically analyzed by using Friedman's Analysis of Variance by Ranks (Zar, 1999).

The ranking analysis is based on measurements from two-dimensional (2D) images of mid-nuclear sections instead of three-dimensional (3D) data sets. With confocal microscopy, fluorophore excitation occurs above and below the plane of focus, resulting in fluorophore bleaching even outside the focal plane (White et al., 2001). Indeed, we observed substantial photobleaching when collecting 3D images for each energid, making quantification of such data sets potentially unreliable. Furthermore, when we performed a sample analysis of measurements from 3D data sets we found greater differences in intensity among different areas compared to the 2D measurements, but the results of the ranking among the three regions remained the same, indicating that our method of measuring the 2D data sets is justified.

Measurement of velocity of sister-chromatid separation in anaphase

High-resolution (1024×1024 pixels) time-lapse recordings were collected with TPLSM settings described above. The recordings were analyzed by using ImageJ (http://rsb.info.nih.gov/ij/) to measure both distance and time elapsed.

Results

Live analyses of the early embryonic cell cycles

We combined histone 2AvD-GFP (histone-GFP) expression with TPLSM to define the duration of the total cell cycle as well as the cell-cycle phases of embryos after cycle 5. Fig. 1A-H illustrate the resolution of TPLSM in terms of both nuclear morphology and timing. In interphase, round nuclei have uniform histone-GFP signal (Fig. 1A,B). Condensation of chromosomes occurs 240 seconds after the onset of interphase, indicating the beginning of prophase (Fig. 1C). We could not define precisely when metaphase begins, because nuclear envelope breakdown cannot be detected with the histone-GFP tag. However, metaphase configurations are clearly recognizable as the condensed chromosomes align along the metaphase plate (Fig. 1D). The onset of anaphase is precisely identified when sister chromatids begin to separate (Fig. 1E). It is difficult to distinguish late anaphase from telophase even though the sister chromatids are further apart (Fig. 1F,G), but the onset of the next interphase is distinguished by the nuclei changing from a teardrop-oval shape to a

round configuration (compare Fig. 1G with 1H). Therefore, with this technique, we can define the beginning of interphase, prophase and anaphase with 10 second accuracy. This enables us to measure precisely not only the length of the total cell cycle, but also the durations of interphase, prophase-metaphase and anaphase-telophase of different cycles.

We analyzed 39 histone-GFP embryos and found that total cell-cycle time steadily increases with every cycle after cycle 7 (Fig. 1I), which is three cycles earlier than previously reported (Foe and Alberts, 1983; Warn and Magrath, 1982; Zalokar and Erk, 1976). Comparing the time of different cell-cycle phases, we found that only interphase increases (Fig. 1I). Other cell-cycle phases were unchanged: prophase-metaphase durations remained about 230 seconds (s.d.=20 seconds) and anaphase-telophase duration about 160 seconds (s.d.=20 seconds). These observations were confirmed by analyses of fixed embryos between cycles 6 and 9 (data not shown).

The interphase extension between cycles 7-10 is not dependent on a DNA replication checkpoint

In wild-type embryos, a depletion of factor(s) involved in DNA replication, may lead to slower DNA replication and longer interphase (S-phase). In DNA-replication checkpoint mutant embryos, such as *grapes* (*grp*) or *Mei-41*, the rapid cycles continued after cycle 11 (Sibon et al., 1997; Sibon et al., 1999). Thus, it has been proposed that interphase extension after cycle 10 depends on proper function of the DNA-replication checkpoint (Nyberg et al., 2002; Sibon et al., 1999; Sibon et al., 1997).

To address whether the DNA-replication checkpoint function accounts for interphase extension before cycle 10, we analyzed grp^1 embryos from grp^1/grp^1; *histone-GFP* mothers with TPLSM. We found that interphase increased from cycle 7 to cycle 10 (Fig. 1J), as in control embryos, indicating that interphase extension between cycle 7 and cycle 10 is DNA-replication checkpoint independent. This observation was confirmed by estimating interphase time in fixed grp^1 embryos (data not shown). It should be noted that interphase duration after cycle 10 in grp^1 embryos extends, but less dramatically than in wild-type embryos (Fig. 1J), confirming previous observations (Sibon et al., 1997; Sibon et al., 1999; Yu et al., 2000).

The preblastoderm cycles are metasynchronous in wild-type embryos

When analyzing fixed wild-type embryos, we observed embryos with nuclei at different cell-cycle phases, indicating metasynchronous mitoses before cycle 10 (e.g. Fig. 2H). Thus, we asked whether nuclei in different regions extend interphase coordinately. To exclude fixation artifacts and to measure cell-cycle phases, we examined live preblastoderm embryos with TPLSM. We determined the cell-cycle phases of nuclei in different regions of single embryos at cycle 7. At this stage, nuclei are spread along the anteroposterior axis. Fig. 2A-F show an embryo with regional differences in cell-cycle phases. We followed two nuclei, one located posteriorly and the other in the middle of the embryo (Fig. 2B). Both entered mitosis (prophase) at the same time (Fig. 2B). Surprisingly, 220 seconds later the posterior nucleus entered anaphase, while the medial one remained in metaphase (Fig. 2C), entering anaphase 40 seconds later (Fig. 2D). Both nuclei were in telophase by 520 seconds (Fig. 2E) and entered the next interphase at the same time (Fig. 2F). Thus, in this particular case, prophase-metaphase of the medial nucleus was 40 seconds longer than that of the more posterior nucleus although interphase showed little regional difference. Similar metasynchrony was observed in all of the nine embryos analyzed at cycle 7. The average prophase-metaphase time of medial nuclei was 20 seconds longer compared with nuclei in the posterior region (P=0.0289; n=9, Fig. 2G). This temporal difference was compensated by a 20 second shorter anaphase-telophase in the middle region so that nuclei entered the next

interphase at similar times (Fig. 2F,G). Therefore, total cell-cycle duration of medial and posterior nuclei were not different (total cell-cycle duration: medial=620±40 seconds, posterior=600±50 seconds, n=9).

Similar regional differences in cell-cycle-phase durations were also observed at cycle 8 (n=17 embryos) (Fig. 2G). Again, prophase-metaphase was 30 seconds longer in the middle region (P=0.0036, n=17) while anaphase-telophase was 20 seconds shorter (P=0.0013, n=17), with the total cell-cycle time remaining similar (total cycle duration: medial=640±70 seconds, posterior=630±80 seconds, n=17). These observations indicate that metasynchronous mitoses in preblastoderm cycles result from different cycle-phase durations.

To confirm these observations, the cell-cycle phases in four different regions (anterior, anterior medial, posterior medial and posterior) of embryos fixed between cycles 5 and 10 were determined. For each cycle, 700 to 1000 fixed embryos were immunostained and analyzed. This method has two advantages over live analysis: the entire embryo is accessible for analyses and all cycle phases can be identified. Between cycles 5 and 8, more metaphase and fewer anaphase nuclei were observed in the two middle regions compared with nuclei at the two polar regions (Fig. 2H), indicating longer metaphase and shorter anaphase in the middle than at the two polar regions. By contrast, there was little or no regional difference in the number of interphase, prophase and telophase nuclei (data not shown), supporting the data from live embryos that difference in metaphase duration between the polar regions and the middle is largely compensated by a concomitant change in anaphase duration. Interestingly, at cycles 9 and 10, cell-cycle phases were more synchronous than earlier cycles (data not shown).

As distances between two daughter nuclei at telophase showed no regional difference, we can assume that sister chromatids migrate the same distance in anaphase. Therefore, we tested whether differences in velocity of sister-chromatid migration in anaphase could account for the regional difference in anaphase-telophase timing (Fig. 2G). As shown in Table 1, between cycles 6 and 8, sister chromatids migrate significantly faster in the middle region of the embryo compared with the posterior region, accounting for the differences in anaphase duration between the regions.

CycB levels around nuclei correlate with metasynchronous mitoses

The previous observations raise the question: what causes the regional difference in timing of cell-cycle phases? Because it has been previously shown that metaphase is longer in preblastoderm embryos with more CycB (Stiffler et al., 1999), we asked whether higher CycB levels around nuclei within an embryo correlated with longer metaphase. We immunostained wild-type embryos at cycle 7 with anti-CycB antiserum and determined CycB levels within an energid, which comprises the nucleus and its associated yolk-free cytoplasmic island (Counce, 1973) (Fig. 3A). For each embryo, CycB immunofluorescence intensities of three energids in anterior (Fig. 3B), middle (Fig. 3C) and posterior (Fig. 3D) regions were measured. To compare the regional differences of CycB level, we ranked the average pixel intensity values in the three regions within each embryo. For prophase, metaphase and anaphase, the rank sum was highest in the middle of the embryo and lowest in the posterior region (Fig. 3E). By contrast, no regional differences were found in either telophase or interphase (Fig. 3E). This indicates that there is more CycB around nuclei in the middle of the embryo at metaphase, correlating with the longer metaphase in this region.

Dosage effects of Cdk1-CycB activity on cell-cycle phases

Although immunocytochemistry can detect local difference of CycB levels, it is not possible to measure regional differences of Cdk1-CycB activity within a living embryo. Therefore, we varied Cdk1-CycB levels in the entire embryo by changing maternal *cycB* gene copy number and then analyzed these embryos for alterations in cell-cycle-phase time using TPLSM. We found that higher CycB levels correlated with longer prophase-metaphase between cycles 6 and 10 (Fig. 4A).

We also examined fixed embryos to further test this dosage effect of CycB on prophase-metaphase duration. Previously, we pooled cell-cycle-phase data between cycle 2 and cycle 8 (Stiffler et al., 1999). However, the observation that interphase duration changes after cycle 7 made it necessary to analyze the cycle phases for each cycle. Because total cell-cycle time is known from live analyses, the mitotic indices determined from fixed embryos can be converted into absolute time (Fig. 4C). We estimated that metaphase in *one cycB* embryos was 35 seconds shorter than in *two cycB* embryos and 62 seconds shorter than in *four cycB* embryos at cycle 7 (Fig. 4C), confirming that metaphase duration is sensitive to CycB levels: more CycB correlates with longer metaphase (P=0.004 based on isotonic regression test (Gaines and Rice, 1990). This effect of CycB on metaphase duration was independent of whether the differences in CycB levels were global (among embryos of different maternal genotypes) or local (regional differences within an embryo).

When we analyzed anaphase-telophase duration in live embryos with more CycB, we did not observe shorter anaphase-telophase as expected (data not shown). It is possible that the time differences are too small to detect among embryos with different amounts of CycB. For this reason, we analyzed fixed embryos. Indeed, we estimated that anaphase in *four cycB* embryos was 5 seconds shorter than in *two cycB* embryos and 13 seconds shorter than in *one cycB* embryos (Fig. 4C). Thus, the longer metaphase in *four cycB* embryos was compensated up to 50% by a shorter anaphase. Varying CycB levels produced incomplete compensation, indicating that anaphase duration is more sensitive to local differences in CycB concentration than global differences. Nevertheless, these results suggest that anaphase duration is affected by differing CycB levels, whether these differences occur within an embryo or among embryos of different maternal genotypes. Perhaps, there are other unknown factors that can also affect anaphase duration.

Interestingly, we found that increased CycB levels correlated with shorter interphase after cycle 7 (Fig. 4B) in live embryos. These observations were confirmed from data calculated from fixed embryos (Fig. 4C). Thus, longer metaphase is almost completely compensated by shorter anaphase and interphase.

Furthermore, interphase extension begins earlier in embryos with less maternal CycB than in those embryos with more CycB (Fig. 4B), supporting the idea that interphase extension occurs when CycB becomes limited (Edgar et al., 1994). A crucial level of CycB would be reached earlier in embryos receiving less maternal CycB.

Velocity of sister chromatid separation in anaphase correlates with CycB levels

We used *one cycB* and *four cycB* embryos to test whether increased amounts of CycB resulted in shorter anaphase time because sister chromatids moved faster. As shown in Table 1, whenever more CycB was present, sister chromatids moved significantly faster, whether the difference of CycB occurred within an embryo or among embryos of different maternal genotypes.

Cell cycle progression after cycle 10

We observed that metasynchrony before cycle 10 resulted from regional differences in metaphase and anaphase time. As metasynchronous mitoses were also observed after cycle 10 (Foe and Alberts, 1983), we asked whether it was also a result of longer metaphases in the middle region of the embryo. We analyzed live embryos with TPLSM and found that nuclei at the two polar regions enter the succeeding blastoderm cycle earlier than nuclei in the middle, confirming observations made by Foe and Alberts (Foe and Alberts, 1983). Surprisingly, we further found that both interphase and total cycle of cycles 11 and 12 were longer in the middle regions than at the posterior poles (Fig. 5A-D), although no regional difference was observed in any other cell-cycle phases. At cycle 11, interphase was 370 seconds in the middle (s.d.=30 seconds) and 350 seconds in the posterior region (s.d.=30 seconds, n=36). At cycle 12, this regional difference increased: interphase was 510 seconds in the middle (s.d.=50 seconds) and 460 seconds in the posterior region (s.d.=50 seconds, n=17, Fig. 5E). Similar observations were made for cycle 13 (data not shown). Thus nuclei in the posterior region entered a blastoderm cycle earlier than nuclei in the middle. With each blastoderm cycle, this regional difference increased, up to a difference of 120 seconds at the beginning of cycle 13. These observations clearly demonstrate that the reason for earlier entry of succeeding blastoderm cycle at the two poles is a lengthening of interphase in the middle region of the embryo.

Discussion

Metasynchronous mitoses before cycle 10: local oscillation of CycB and global cytoplasmic flow during axial expansion

Prior to cycle 10, regional differences in timing of cell-cycle progression are due to changes in metaphase and anaphase duration, but not interphase duration, as it is after cycle 10. Thus, the metasynchronous mitoses before and after cycle 10 are probably generated by different mechanisms. Our findings that local differences of CycB levels correlate with metasynchronous mitoses in the preblastoderm cycles raise the question: how are higher CycB levels in the middle of the embryo generated during each prophase and anaphase of cycles 4-8? During these cycles, we observed a gradual decline of CycB in the interior of the embryo. Between late interphase and early anaphase of cycle 4 to cycle 8, cytoplasm in the interior, containing less CycB, flows towards the polar regions (Baker et al., 1993). This cytoplasmic movement may cause slightly lower CycB levels at the polar regions during metaphase and anaphase. Meanwhile, cytoplasm at the cortical region with more CycB flows in an opposite direction towards the anterior-medial region and then moves slightly inward (Fig. 6B,C) (von Dassow and Schubiger, 1994). Therefore, we propose that the inward cytoplasmic flow might cause the temporal and local increase of CycB observed in the middle region of the embryo from prophase to anaphase.

A model to explain the axial expansion process (between cycle 4 and cycle 8) is based on solation-contraction of the microfilament network within the embryo (for details, see von Dassow and Schubiger, 1994). Briefly, according to this model, local solation (disassembly) of the contractile microfilament network in the center of embryo will cause the microfilament network attached to the cortex to contract away from the solated site in the center of the embryo. Nuclei and cytoplasm in the center of the embryo move towards the two polar regions because the tension generated by the contraction of the microfilament network is greatest along the anteroposterior axis (von Dassow and Schubiger, 1994). This poleward cytoplasmic movement in the interior would force cortical material to flow from poles towards the middle region, where the cytoplasm then moves inwards. This then generates two circular cytoplasmic movement during prophase and metaphase (Fig. 6B,C). However, the nature of the ‘solating agent’ remains unknown in this model (von Dassow

and Schubiger, 1994). We observed that Cdk1-CycB affects both microtubule and microfilament dynamics (Ji et al., 2002) and that CycB is higher in the middle region from prophase to anaphase (Fig. 3E), suggesting that Cdk1-CycB is a likely candidate for the solating agent that initiates axial expansion. Therefore, we see a positive feedback loop between CycB distribution and cytoplasmic flow (Fig. 6). This feedback loop is disrupted by CycB degradation at anaphase, when we observe a slight backward cytoplasmic flow.

According to this scenario, the global cytoplasmic movement and local oscillation of mitotic cyclin concentration are the two key factors generating metasynchronous mitoses during preblastoderm cycles. Interestingly, axial expansion only occurs between cycle 4 and 8 (Baker et al., 1993), the same period during which we observe regional differences in metaphase and anaphase duration. This global cytoplasmic movement is not observed after cycle 8, correlating with the observation of little regional difference in metaphase and anaphase duration after cycle 8. Direct observation of CycB movement in embryos with CycB-GFP fusion proteins (Huang and Raff, 1999) would be ideal. However, we were unable to detect CycB-GFP signal prior to cycle 10.

Different control mechanisms of interphase extension before and after cycle 10

Interphase extension after cycle 10 has been explained in two ways. Edgar et al. (Edgar et al., 1994) observed that decreasing CycB correlates with longer interphase after cycle 10, thus proposed that interphase extension after cycle 10 was due to CycB limitation. However, based on the observation that fast cycles continue after cycle 10 in *grp* mutant embryos, Sibon et al. (Sibon et al., 1997) proposed that in wild-type embryos depletion of factors involved in DNA replication causes longer interphase after cycle 10 and the interphase extensions are regulated by the DNA-replication checkpoint pathway.

Several of our observations might resolve this controversy. We report here that interphase extension occurs in *grp* mutant embryos before cycle 10 (Fig. 1J), thus we propose that interphase extension before cycle 10 is solely due to CycB limitation. This is further supported by the following observations. First, interphase extension occurs at an earlier cycle when maternal CycB is reduced and later when CycB is increased (Fig. 4B). Second, looking within a specific cycle, interphase is longer when CycB is lower and shorter when CycB is higher (Fig. 4B,C). Third, global CycB levels start to oscillate at the beginning of cycle 6 or 7 in wild-type embryos (Edgar et al., 1994), exactly the same time when interphase duration starts to increase (Fig. 1I).

We also propose that after cycle 10, interphase extension is under control of both CycB limitation and the DNA-replication checkpoint. It was reported that grp^1 is a null allele (Fogarty et al., 1997). We observed that interphase continuously extends in grp^1 embryos after cycle 10, although this extension is not as extensive as in wild-type embryos (Fig. 1J). This observation supports the idea that limitation of CycB is responsible for this increase.

With these two proposals in mind, we re-examined the interphase extension. Before cycle 10, interphase extension occurs coordinately in all nuclei and the nuclei doubling time shows no regional difference. After cycle 10, nuclei divide slower in the middle because interphase in this region is longer, which correlate with an increase of nuclear density in this region of the embryo after cycle 10 (Blankenship and Wieschaus, 2001) (G. K. Yasuda, PhD thesis, University of Washington, 1992). In many organisms, a higher nucleocytoplasmic ratio correlates with a slower cell cycle (Sveiczer et al., 2001). A venerable hypothesis is that higher nuclear density could result in an earlier depletion of factors necessary for DNA replication, such as deoxynucleotide triphosphates. This may result in slower DNA replication, thereby specifically prolonging interphase and ultimately total cell-cycle length.

How do Cdk1-CycB levels affect the velocity of sister chromatid separation?

Currently, there are two major mechanisms proposed to regulate sister chromatid separation in anaphase. First, disassembly of microtubules in kinetochore regions shortens kinetochore microtubules and generates the force that pulls the sister chromatids apart once cohesin is cleaved by separase (Compton, 2002). Second, the disassembly of spindle microtubules at the centrosomal region induces the poleward microtubule movement, which then generates the force that separates the sister chromatids (Compton, 2002). In syncytial blastoderm *Drosophila* embryos (cycles 10 to 13), it has been documented that the poleward microtubule movement is the key component that separate the sister chromatids in anaphase A, whereas the disassembly of microtubules at the kinetochore is a minor factor (Maddox et al., 2002).

How does Cdk1-CycB affect velocity of sister chromatid separation? We have shown that CycB levels negatively affect microtubule stability: higher Cdk1-CycB levels lead to less stable microtubules and, correspondingly, lower Cdk1-CycB levels lead to more stable microtubules (Stiffler et al., 1999; Ji et al., 2002). It also takes a longer time to form a stable metaphase configuration when CycB levels are elevated. Furthermore, when more CycB is present the microtubules of the metaphase spindle are weaker than when less CycB is available. We speculate that the disassembly of spindle microtubule is faster or more efficient at the centrosomal regions because there are fewer microtubules at the centrosomal regions in embryo with higher Cdk1-CycB activity (Stiffler et al., 1999), contributing to the faster poleward microtubule movement. Alternatively, Cdk1-CycB might affect the sister chromatid movement via its target proteins in the centrosomal regions and/or the midzone where the interpolar microtubules overlap. For example, Cdk1-CycB phosphorylates p93dis1, which is enriched in the centrosomal regions (Nabeshima et al., 1995) and kinesin Eg5 (*Drosophila* homolog KLP61F), which accumulates on the midzone after phosphorylation (Blangy et al., 1995; Sawin and Mitchison, 1995; Sharp et al., 1999). Mutation of p93dis1 in fission yeast results in failure in sister chromatid separation (Nabeshima et al., 1995), while the phosphorylated bipolar kinesin KLP61F is thought to be involved in sister chromatid separation by regulating sliding of the interpolar microtubules in anaphase (Sharp et al., 1999).

Our observation that Cdk1-CycB affects the velocity of sister chromatid movement during anaphase supports the idea that microtubule dynamics contribute to the mechanical force for sister chromatid separation. This novel observation provides an entry point to further investigate the molecular mechanism that leads to disassembly of spindle microtubules by analyzing, for example, the possible functions of the target proteins of Cdk1-CycB in the centrosomal region.

Limitations and opportunities using the TPLSM

The TPLSM provides new opportunities for precisely analyzing the timing of biological events (Squirrell et al., 1999). Its major advantages over conventional confocal imaging are that the two-photon excitation generates less photo damage to thick living objects, and is particularly successful at imaging fluorescent signals deep in the specimen (Centonze and White, 1998; Squirrell et al., 1999; White et al., 2001). Indeed, we found that with traditional confocal microscopy, GFP signals prior to cycle 10 were difficult to detect. In addition, we frequently observed cell-cycle arrest and chromosome bridges in the region of focus, indicating phototoxic effects, confirming the observations made by others (Clarkson and Saint, 1999).

Using TPLSM, we found that in the earliest embryonic stages, an abundance of many maternal proteins obscure the observation of the product at the target. However, after the

first few cycles, depending on the protein, the maternal storage declines and the GFP signal from the fusion protein becomes target specific. The time point of detection depends on the localization, the amount and function of the protein. For example, histone-GFP on chromosome is recognized after cycle 4, while tubulin-GFP can only be recognized on microtubules after cycle 8 (J.-Y.J., J.M.S. and G.S., unpublished).

The ability to detect fluorescent label within the preblastoderm embryo and follow changes in this signal over a relatively long period of time without affecting viability provides opportunity to study this early developmental stage that has been previously inaccessible. For example, there are an abundance of maternal effect mutations that develop apparently normal up to cycle 5 or 6, after which development arrests, a phenomenon referred to as ‘epigenetic crisis’ (Counce, 1973). This phenomenon is observed in many vertebrates and invertebrates, indicating that mid-cleavage is a critical developmental stage (Counce, 1973). Although some of the *Drosophila* mutations have been molecularly identified, a phenotypic analysis using the TPLSM to assess the function of these genes will increase our understanding of this developmentally critical period.

Acknowledgments

We thank Christian Lehner, Jordan Raff, Rob Saint and Bill Sullivan for providing mutant fly stocks, and Will Whitfield and David Glover for anti-CycB antiserum (Rb271). We are especially grateful to John G. White for allowing us to use the two-photon microscope in his laboratory. We thank Todd Clason, Kevin Eliceiri, Charles Thomas and Haining Zhang for their help with the TPLSM and computer analysis. We appreciate Ray Huey’s advice on statistical analyses and encouragement throughout this project, and we also thank Pat O’Farrell, Margrit Schubiger, members in the Schubiger laboratory and the anonymous reviewers for their very helpful comments with the manuscript. This work was supported by NSF grant IBN 97-27944 and NIH grant GM58282 to G.S.

References

Baker J, Theurkauf WE, Schubiger G. Dynamic changes in microtubule configuration correlate with nuclear migration in the preblastoderm *Drosophila* embryo. J. Cell Biol. 1993; 122:113–121. [PubMed: 8314839]

Blangy A, Lane HA, d’Herin P, Harper M, Kress M, Nigg EA. Phosphorylation by p34cdc2 regulates spindle association of human Eg5, a kinesin-related motor essential for bipolar spindle formation in vivo. Cell. 1995; 83:1159–1169. [PubMed: 8548803]

Blankenship JT, Wieschaus E. Two new roles for the Drosophila AP patterning system in early morphogenesis. Development. 2001; 128:5129–5138. [PubMed: 11748148]

Centonze VE, White JG. Multiphoton excitation provides optical sections from deeper within scattering specimens than confocal imaging. Biophys. J. 1998; 75:2015–2024. [PubMed: 9746543]

Clarkson M, Saint R. A His2AvDGFP fusion gene complements a lethal His2AvD mutant allele and provides an in vivo marker for *Drosophila* chromosome behavior. DNA Cell Biol. 1999; 18:457–462. [PubMed: 10390154]

Compton DA. Chromosome segregation: pulling from the poles. Curr. Biol. 2002; 12:R651–R653. [PubMed: 12361583]

Counce, SJ. The causal analysis of insect embryogenesis. In: Counce, SJ.; Waddington, CH., editors. Developmental Systems: Insects. Academic Press; London, New York: 1973. p. 1-156.

Edgar BA, Datar SA. Zygotic degradation of two maternal Cdc25 mRNAs terminates *Drosophila*’s early cell cycle program. Genes Dev. 1996; 10:1966–1977. [PubMed: 8756353]

Edgar BA, Kiehle CP, Schubiger G. Cell cycle control by the nucleo-cytoplasmic ratio in early *Drosophila* development. Cell. 1986; 44:365–372. [PubMed: 3080248]

Edgar BA, Sprenger F, Duronio RJ, Leopold P, O’Farrell PH. Distinct molecular mechanism regulate cell cycle timing at successive stages of *Drosophila* embryogenesis. Genes Dev. 1994; 8:440–452. [PubMed: 7510257]

Foe VE, Alberts BM. Studies of nuclear and cytoplasmic behavior during the five mitotic cycles that precede gastrulation in *Drosophila* embryogenesis. J. Cell Sci. 1983; 61:31–70. [PubMed: 6411748]

Foe, VE.; Odell, GM.; Edgar, BA. Mitosis and morphogenesis in the *Drosophila* embryo: point and counterpoint. In: Bate, M.; Arias, AM., editors. The Development of Drosophila melanogaster. Cold Spring Harbor Laboratory Press; New York: 1993. p. 149-300.

Fogarty P, Campbell SD, Abu-Shumays R, Phalle BS, Yu KR, Uy GL, Goldberg ML, Sullivan W. The *Drosophila grapes* gene is related to checkpoint gene *chk1/rad27* and is required for late syncytial division fidelity. Curr. Biol. 1997; 7:418–426. [PubMed: 9197245]

Gaines SD, Rice WR. Analysis of biological data when there are ordered expectations. Am. Nat. 1990; 135:310–317.

Hendzel MJ, Wei Y, Mancini MA, van Hooser A, Ranalli T, Brinkley BR, Bazett-Jones DP, Allis CD. Mitosis-specific phosphorylation of histone H3 initiates primarily within pericentromeric heterochromatin during G2 and spreads in an ordered fashion coincident with mitotic chromosome condensation. Chromosoma. 1997; 106:348–360. [PubMed: 9362543]

Huang JY, Raff JW. The disappearance of cyclin B at the end of mitosis is regulated spatially in *Drosophila* cells. EMBO J. 1999; 18:2184–2195. [PubMed: 10205172]

Jacobs HW, Knoblich JA, Lehner CF. *Drosophila* Cyclin B3 is required for female fertility and is dispensable for mitosis like Cyclin B. Genes Dev. 1998; 12:3741–3751. [PubMed: 9851980]

Ji JY, Haghnia M, Trusty C, Goldstein LS, Schubiger G. A genetic screen for suppressors and enhancers of the *Drosophila* Cdk1-Cyclin B identifies maternal factors that regulate microtubule and microfilament stability. Genetics. 2002; 162:1179–1195. [PubMed: 12454065]

Kirschner M, Newport J, Gerhart J. The timing of early developmental events in *Xenopus*. Trends Genet. 1985; 1:41–47.

Maddox P, Desai A, Oegema K, Mitchison TJ, Salmon ED. Poleward microtubule flux is a major component of spindle dynamics and anaphase A in mitotic *Drosophila* embryos. Curr. Biol. 2002; 12:1670–1674. [PubMed: 12361570]

Morgan DO, Roberts JM. Oscillation sensation. Nature. 2002; 418:495–496. [PubMed: 12152065]

Murray AW. Remembrance of things past. Nature. 1991; 349:367–368. [PubMed: 1825129]

Murray AW, Kirschner MW. What controls the cell cycle? Sci. Am. 1991; 264:56–63. [PubMed: 1828616]

Nabeshima K, Kurooka H, Takeuchi M, Kinoshita K, Nakaseko Y, Yanagida M. p93dis1, which is required for sister chromatid separation, is a novel microtubule and spindle pole body-associating protein phosphorylated at the Cdc2 target sites. Genes Dev. 1995; 9:1572–1585. [PubMed: 7628693]

Newport J, Kirschner M. A major developmental transition in early *Xenopus* embryos: I. characterization and timing of cellular changes at the midblastula stage. Cell. 1982; 30:675–686. [PubMed: 6183003]

Nyberg KA, Michelson RJ, Putnam CW, Weinert TA. Toward maintaining the genome: DNA damage and replication checkpoints. Annu. Rev. Genet. 2002; 36:617–656. [PubMed: 12429704]

Pritchard DK, Schubiger G. Activation of transcription in *Drosophila* embryos is a gradual process mediated by the nucleocytoplasmic ratio. Genes Dev. 1996; 10:1131–1142. [PubMed: 8654928]

Rabinowitz M. Studies on the cytology and early embryology of the egg in *Drosophila melanogaster*. J. Morphol. 1941; 69:1–49.

Sawin KE, Mitchison T,J. Mutations in the kinesin-like protein Eg5 disrupting localization to the mitotic spindle. Proc. Natl. Acad. Sci. USA. 1995; 92:4289–4293. [PubMed: 7753799]

Schubiger G, Edgar B. Using inhibitors to study embryogenesis. Methods Cell Biol. 1994; 44:697–713. [PubMed: 7707976]

Sharp DJ, McDonald KL, Brown HM, Matthies HJ, Walczak C, Vale RD, Mitchison TJ, Scholey JM. The bipolar kinesin, KLP61F, cross-links microtubules within interpolar microtubule bundles of *Drosophila* embryonic mitotic spindles. J. Cell Biol. 1999; 144:125–138. [PubMed: 9885249]

Shermoen AW, O'Farrell PH. Progression of the cell cycle through mitosis leads to abortion of nascent transcripts. Cell. 1991; 67:303–310. [PubMed: 1680567]

Sherr CJ. Cancer cell cycles. Science. 1996; 274:1672–1677. [PubMed: 8939849]

Sibon OC, Stevenson VA, Theurkauf WE. DNA-replication checkpoint control at the *Drosophila* midblastula transition. Nature. 1997; 388:93–97. [PubMed: 9214509]

Sibon OC, Laurencon A, Hawley R, Theurkauf WE. The *Drosophila* ATM homologue *Mei-41* has an essential checkpoint function at the midblastula transition. Curr. Biol. 1999; 9:302–312. [PubMed: 10209095]

Squirrell JM, Wokosin DL, White JG, Bavister BD. Long-term two-photon fluorescence imaging of mammalian embryos without compromising viability. Nat. Biotechnol. 1999; 17:763–767. [PubMed: 10429240]

Stiffler LA, Ji JY, Trautmann S, Trusty C, Schubiger G. Cyclin A and B functions in the early *Drosophila* embryo. Development. 1999; 126:5505–5513. [PubMed: 10556074]

Su TT, Sprenger F, DiGregorio PJ, Campbell SD, O'Farrell PH. Exit from mitosis in *Drosophila* syncytial embryos requires proteolysis and cyclin degradation, and is associated with localized dephosphorylation. Genes Dev. 1998; 12:1495–1503. [PubMed: 9585509]

Sullivan W, Fogarty P, Theurkauf W. Mutations affecting the cytoskeletal organization of syncytial *Drosophila* embryos. Development. 1993; 118:1245–1254. [PubMed: 8269851]

Sveiczer A, Tyson JJ, Novak B. A stochastic, molecular model of the fission yeast cell cycle: role of the nucleocytoplasmic ratio in cycle time regulation. Biophys. Chem. 2001; 92:1–15. [PubMed: 11527575]

Thomas C, DeVries P, Hardin J, White JG. Four-dimensional imaging: computer visualization of 3D movements in living specimens. Science. 1996; 273:603–607. [PubMed: 8662545]

von Dassow G, Schubiger G. How an actin network might cause fountain streaming and nuclear migration in the syncytial *Drosophila* embryo. J. Cell Biol. 1994; 127:1637–1653. [PubMed: 7798318]

Warn RM, Magrath R. Observations by a novel method of surface changes during the syncytial blastoderm stage of the *Drosophila* embryo. Dev. Biol. 1982; 89:540–548. [PubMed: 6799345]

Wei Y, Yu L, Bowen J, Gorovsky MA, Allis CD. Phosphorylation of histone H3 is required for proper chromosome condensation and segregation. Cell. 1999; 97:99–109. [PubMed: 10199406]

White JG, Squirrell JM, Eliceiri KW. Applying multiphoton imaging to the study of membrane dynamics in living cells. Traffic. 2001; 2:775–780. [PubMed: 11733043]

Whitfield W, Gonzalez C, Maldonado-Codina G, Glover D. The A- and B-type cyclins of *Drosophila* are accumulated and destroyed in temporally distinct events that define separable phases of the G2-M transition. EMBO J. 1990; 9:2563–2572. [PubMed: 2142452]

Wokosin DL, Squirrell JM, Eliceiri KW, White JG. Optical workstation with concurrent, independent multiphoton imaging and experimental laser microbeam capabilities. Rev. Sci. Instrum. 2003; 74:1–9.

Yasuda GK, Schubiger G. Temporal regulation in the early embryo: is MBT too good to be true? Trends Genet. 1992; 8:124–127. [PubMed: 1631954]

Yu KR, Saint RB, Sullivan W. The Grapes checkpoint coordinates nuclear envelope breakdown and chromosome condensation. Nat. Cell Biol. 2000; 2:609–615. [PubMed: 10980701]

Zalokar M, Erk I. Division and migration of nuclei during early embryogenesis of *Drosophila melanogaster*. J. Microscopie Biol. Cell. 1976; 25:97–106.

Zar, JH. Biostatistical Analysis. 4th edn. Prentice Hall; NJ: 1999.

Zou H, McGarry TJ, Bernal T, Kirschner MW. Identification of a vertebrate sister-chromatid separation inhibitor involved in transformation and tumorigenesis. Science. 1999; 285:418–422. [PubMed: 10411507]

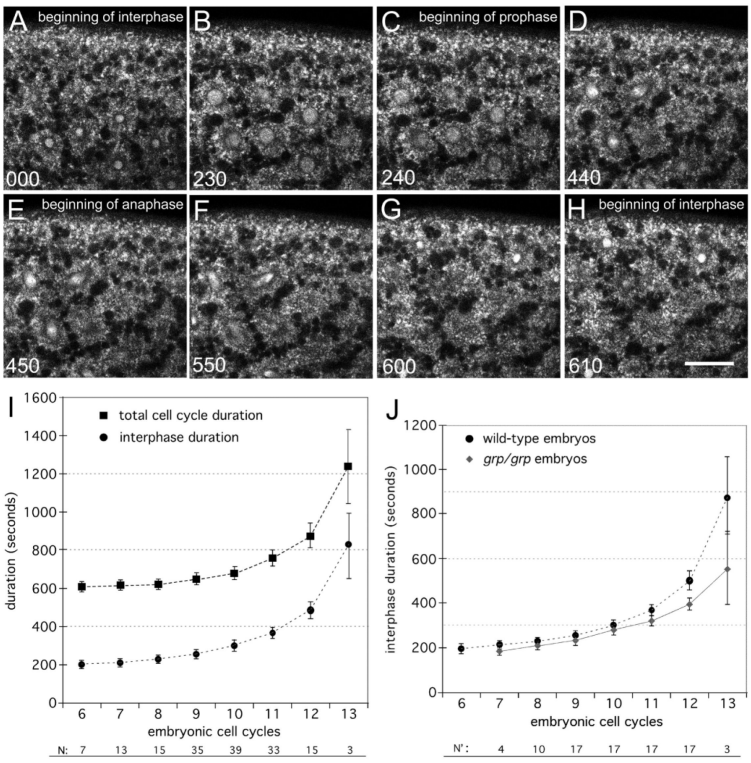

Fig. 1.

Live analyses of cell-cycle durations of *histone-GFP* embryos between cycles 6 and 13. (A-H) Different cycle phases of an embryo at cycle 8. (A) The earliest interphase (000 seconds); (B) last interphase image recorded (230 seconds). Ten seconds later (C), nuclei are in prophase, which is characterized by punctuated GFP signal and loss of the round nuclear morphology. At 440 seconds (D), an obvious metaphase configuration is established and 10 seconds later sister chromatids begin to separate (E), indicating the beginning of anaphase. Between 550 and 600 seconds, nuclei progress from anaphase (F, clear teardrop shape) to telophase (G, more rounded). Ten seconds later (H, 610 seconds), the beginning of interphase of cycle 9 is observed. With this information, we calculated durations of total cell cycles, interphases, prophase-metaphases and anaphase-telophases between cycles 6 and 13. (I) Overall cell-cycle and interphase duration between cycles 6 and 13, based on time-lapse recordings of 39 embryos. For each cycle, number of embryos (N) differs because the quality of recordings improves after cycle 5; before cycle 5, abundant maternal loading of histone-GFP obscures the chromosomal histone-GFP. All data points are aligned at cycle 9, when nuclei migrate to the cortex and pole buds are formed (Foe and Alberts, 1983). Because the preblastoderm cycles are not exactly synchronous (Fig. 2), cell-cycle-phase duration within each cycle was defined as the average of 1-2 nuclei in the middle with 1-2 nuclei in the posterior region of each embryo. (J) Interphase durations of *grp*^{1} embryos do not differ from wild-type embryos before cycle 11. The number of *grp*^{1} embryos (N') is shown in J; data for wild-type embryos are taken from I. Scale bar: 30 μm.

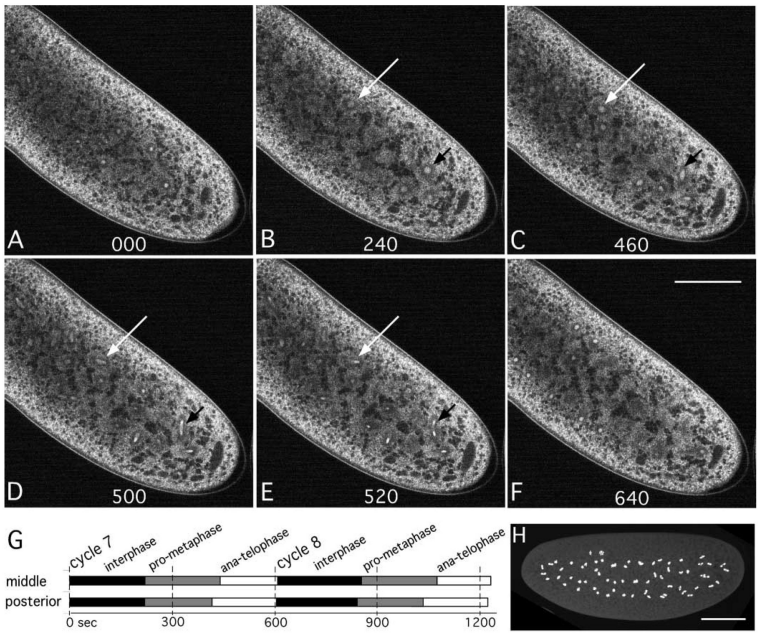

Fig. 2.

Metasynchronous mitoses occur prior to cycle 10. (A-F) are images from a time-lapse recording of a histone-GFP embryo at cycle 7. All nuclei are at the beginning of interphase (A) and then enter prophase (B). (C) The nucleus in the posterior region enters anaphase (black arrow), while the one in the middle (white arrow) remains in metaphase and enters anaphase 40 seconds later (D). (E) Both nuclei are in telophase. The two daughter nuclei in (E) moved out of the focal plane but all other nuclei show early interphase configuration of cycle 8 at the same time (F). That nuclei in different regions enter interphase at the same time is supported from other time-lapse recordings. (G) Summary of the regional differences of cell-cycle-phase durations in histone-GFP embryos at cycle 7 (n=9) and cycle 8 (n=17), showing that prophase-metaphase is longer and anaphase-telophase is shorter in the middle region than in the posterior region. The total cell cycle time at cycle 8 is not significantly different in the two regions. (H) An epifluorescence image showing metasynchronous mitoses at cycle 7 from a fixed wild-type embryo: nuclei at the two polar regions are in anaphase, whereas the nuclei in the middle region are in metaphase. Scale bars: 100 μm.

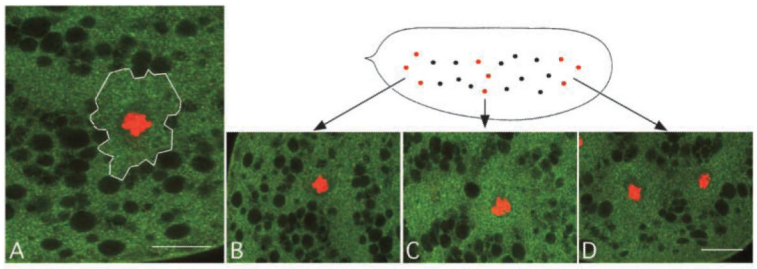

Average pixel intensity of CycB staining: 85.0 ± 4.1 94.6 ± 3.7 74.4 ± 6.3

Rank: 2 3 1

E

Cell-cycle phases	Rank sum of CycB levels in different regions at cycle 7			Number of embryos analyzed	
	Anterior	Middle	Posterior		
interphase	27	23	26	11	
prophase	19	24	11	9	*
metaphase	33	39	18	15	*
anaphase	22	34	16	12	*
telophase	29	28	27	14	

Fig. 3.

Immunostaining and quantification of CycB. (A-D) Wild-type embryos were stained with both anti-CycB (green) and anti-histone H1 (red) antibodies. (A) An energid is outlined and the average pixel intensity within the energid (green channel only) was measured. The outline was defined by taking the shortest distance between yolk granules (black) around the nucleus. Because the average pixel intensities (total pixel numbers within an area divided by the area) were compared, the exact outlines were not crucial for the comparison. (B-D) CycB levels were quantified from three regions (anterior, middle and posterior) in each embryo, averaging the data from three nuclei in each region. In this example, the mean value of the average pixel intensity of the CycB signal was ranked, with the lowest CycB level (74.4±6.3) as 1, the highest (94.6±3.7) as 3 and the middle (85.0±4.1) as 2. (E) Summary of the rank sum of different cell-cycle phases at cycle 7. The asterisks indicate that the regional difference is statistically significant (P<0.04) based on Friedman's Analysis of Variance by Ranks (Zar, 1999). Scale bars: 20 μm.

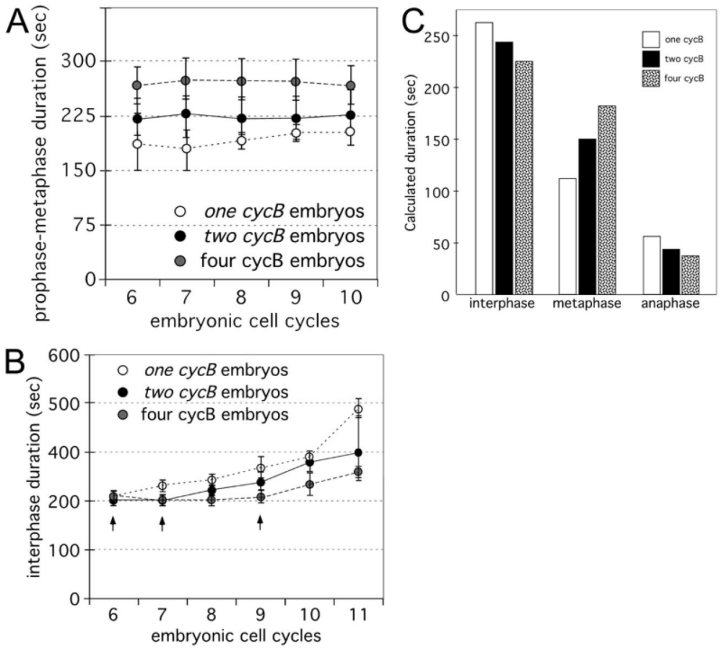

Fig. 4.

Timing of cell-cycle phases are sensitive to varying amounts of CycB. Prophasemetaphase (A) and interphase durations (B) in *one cycB*, *two cycB* and *four cycB* embryos determined from live embryos. For each genotype, 15 to 18 embryos were analyzed. Arrows in B refer to the specific cycle when interphase becomes longer: cycle 6 for *one cycB* embryos, cycle 7 for *two cycB* embryos and cycle 9 for *four cycB* embryos. (C) Estimated durations of interphase, metaphase and anaphase of wild-type embryos at cycle 7 based on fixed embryos (n=333 for *one cycB* embryos, n=915 for *two cycB* embryos and n=501 for *four cycB* embryos).

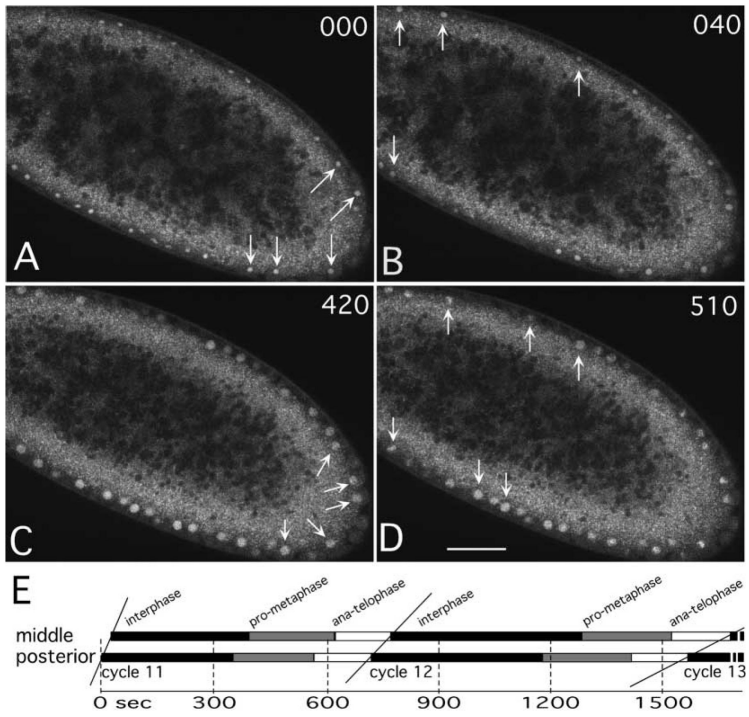

Fig. 5.

Metasynchronous mitoses in blastoderm cycles. TPLSM images of a live embryo showing that, at cycle 12, interphase is longer in the middle region than at the posterior pole. Nuclei at the posterior region enter interphase (A, arrows) 40 seconds earlier than nuclei in the middle region (B, arrows). (C) Nuclei at the posterior region enter prophase, whereas nuclei in the middle enter prophase 90 seconds later (D). In this particular embryo, interphase in the middle region is 50 seconds longer than in the posterior region. (E) Mean values of regional differences of cell-cycle-phase durations in histone-GFP embryos at cycle 11 (n=36) and cycle 12 (n=17), showing that interphase and total cycle are longer in the middle region than the posterior region. Scale bar: 50 μm.

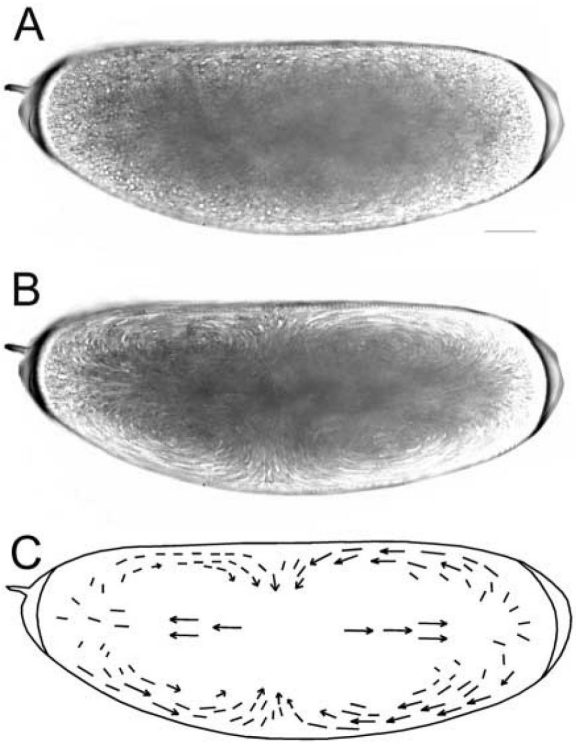

Fig. 6.

Cytoplasmic flow, as indicated by traces of particle movement, during axial expansion (cycle 4 to cycle 8) may contribute to uneven distribution of CycB within an embryo. Both A and B are projections of three-minute time-lapse recordings every 10 seconds of a wild-type embryo at cycle 6. These bright-field transmission images were recorded on a two-photon optical workstation (Wokosin et al., 2003). There is little particle movement in interphase [A, see Baker et al. (Baker et al., 1993) for staging]. By contrast, dramatic particle movement can be observed between interphase and anaphase [B, see Baker et al. (Baker et al., 1993) for staging]. Note the inward flow in the middle region. (C) The direction of the flow in prophase and metaphase. Scale bar: 50 μm.

Table 1

Velocity of sister chromatid separation in anaphase is sensitive to the amount of maternal CycB

Maternal genotype	Average velocity* (μm/min)	s.d.	Middle region			Posterior region			Number of embryos
			Velocity (μm/min)	s.d	Number of measurements	Velocity (μm/min)	s.d.	Number of measurements	
one cycB †	7.40	0.58	7.85	0.38	26	6.97	0.40	26	14
two cycB †	8.17	0.61	8.61	0.45	42	7.81	0.46	51	17
four cycB †	8.75	0.53	9.07	0.40	34	8.51	0.49	45	18

*The differences among *one cycB*, *two cycB* and *four cycB* are highly significant [$P<0.0001$ based on the isotonic regression test (Gaines and Rice, 1990)].

†The regional differences in *one cycB*, *two cycB* and *four cycB* embryos are highly significant ($P<0.0001$ based on one-tailed *t*-test).